Hindawi
Geofluids
Volume 2019, Article ID 8541959, 16 pages
https://doi.org/10.1155/2019/8541959

Research Article

Structural Response of the Metro Tunnel under Local Dynamic Water Environment in Loess Strata

Junling Qiu[1], **Yiwen Qin**[1], **Jinxing Lai**[1], **Ke Wang**[2], **Fangyuan Niu**[3], **Hao Wang**[4], **and Guanglong Zhang**[5]

[1]*School of Highway, Chang'an University, Xi'an 710064, China*
[2]*State Key Laboratory of Rail Transit Engineering Informatization, China Railway First Survey and Design Institute Group Co. Ltd., Xi'an, Shaanxi 710043, China*
[3]*China State Construction Silkroad Construction Investment Group Co., Ltd., Xi'an, Shaanxi 710068, China*
[4]*School of Civil & Construction Engineering, Oregon State University, 101 Kearney Hall, Corvallis, OR 97331, USA*
[5]*Shandong Academy of Building Research, Ji'nan 250031, China*

Correspondence should be addressed to Jinxing Lai; laijinxing@chd.edu.cn

Received 20 March 2018; Accepted 8 August 2018; Published 11 February 2019

Academic Editor: Xueyu Pang

The reasons, prevention, and control of loess disaster are of great concern in practice. In recent years, Xi'an city, China, has taken the leadership in large-scale construction of subway lines in the loess strata. To study the structural response of the tunnel in loess region under local hydrodynamic environment, an experimental testing in 1g as well as a numerical simulation were performed, in which the achieved results were verified and were found to be in good agreement. Furthermore, the results showed that when the water outlet point is above the lining, the overall stress of the lining is "peanut shell," as the water pressure of the outlet point decreases, the tensile stress of the top and bottom of the lining increases, while the compressive stress on both sides decreases; the channel form of the flow to the lining changes with the variation of the position of the water outlet point. It is worth mentioning that in the process of water gushing, the closer to the water source, the greater surface subsidence is, and there is a positive correlation between water pressure and surface subsidence. This study is of significant benchmark for the construction, maintenance, and prevention of tunnel in loess strata under the influence of water environment.

1. Introduction

In the 1840s, Lyell studied sediment deposits along the Mississippi River in the middle of the United States and initially proposed the academic term "Loess" [1]. Compared with other soil, the loess has special structural and water sensitivity: (1) the joint fissure is developed, the mesoscopic structure is porous, and the difference of dry and wet strength is remarkable; (2) most of them have strong collapsibility, softening, and deforming in water [2–6]. Therefore, the change of water environment is very easy to induce engineering geological hazard, and the effect of humankind engineering activity can easily increase the disaster of loess [7–13]. In the past 10 years, Xi'an city, as a main developing city in Western China, has taken the leadership in large-scale construction of subway in the loess strata [14, 15]. On the one hand, according to the situation of Xi'an subway planning, most of the upper layers of subway construction are new loess which have physical features such as high void ratio, incomplete consolidation, and low strength [16–22]. On the other hand, there are lots of ground fissures in Xi'an, so the disturbance of tunnel construction will inevitably lead to large strata deformation [23–27]. During the deformation process, the leakage of urban pipelines will easily lead to large-scale collapsibility of loess strata.

In recent years, on the one hand, scholars in related fields took soak infiltration as the main condition of the experiment and analyzed the mechanism of the catastrophe of subway tunnel project in the groundwater depression cone area and the effect of leakage range of pipeline on the deformation

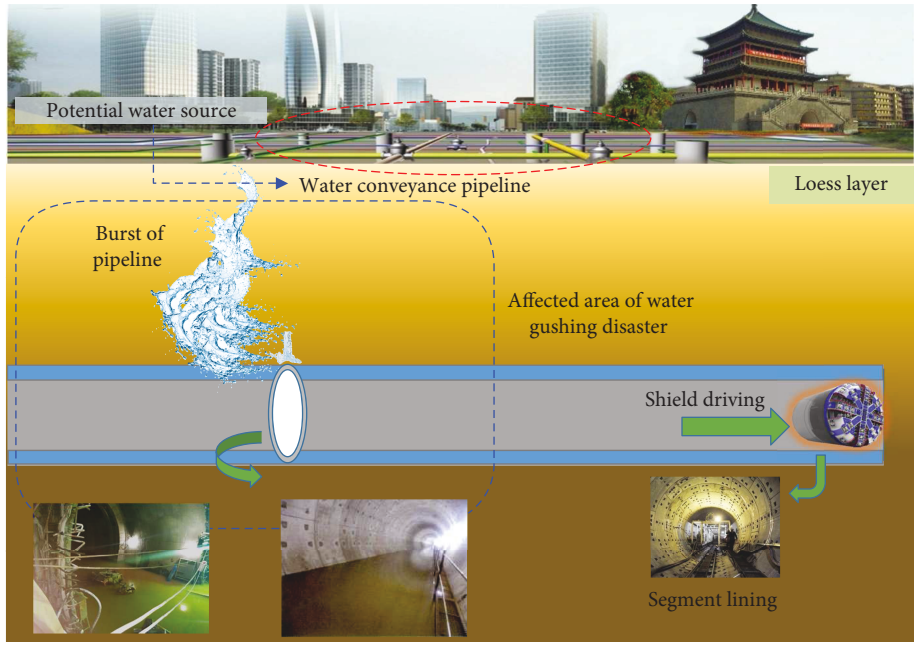

Figure 1: Sketch map of water gushing at site.

and failure of tunnel surrounding rock [28–32]. According to the influence of water leakage at different parts of the tunnel on the surrounding soil and the parallel tunnel, the critical gap width of disaster caused by soil loss was proposed [33–38]. On the other hand, in view of the engineering properties of different rocks and soil under the influence of water, different analytical methods have been used to carry out research: in the clay stratum, the researchers used the homogeneous permeation theory to analyze the effect of long-term seepage of subway tunnel in soft soil area on tunnel and surface subsidence [39–43]; in karst tunnel, researchers carried out model experiments to reveal the catastrophic characteristics of water inrush in the filling karst pipeline and summarized the general characters of the water inrush structure of the rock tunnels [44–48]; in the loess stratum, the researchers through on-site monitoring, radar detection, numerical analysis, and other methods analyzed the damage to the segment structure of the subway water gushing and got the deformation characteristics of the segment structure in the process of water gushing and the distribution laws of the crack and the dislocation of the pipe [49–55].

The mentioned research is mostly concerned with the clay and sandy stratum, and the main condition of the experiment is soak infiltration. Research on water gushing mechanism of subway tunnel in collapsible loess strata involves less, such as the temporal and spatial law of structural damage of the subway tunnel under local dynamic water and mechanical formation mechanism of the water gushing channel in the loess stratum. To study the structural response and damage evolution of tunnel in loess region under local hydrodynamic environment, the water gushing disaster of a section tunnel on Xi'an Metro Line 4 is taken into account as a case study, using experimental testing in 1g and numerical simulation to verify each other, the key analyzed the variation law of pore water pressure, vertical stress of surrounding rock, the strain of lining, and surface settlement, providing a theoretical reference for the construction, maintenance, and prevention of tunnel in loess strata under the influence of water environment.

2. Experiment

2.1. General Situation of Engineering. The preliminary investigation of Xi'an Metro Line 4 showed that there was a large-area collapse loess with large thickness at the southern section of the line, which the maximum thickness of collapse loess layer was within 25 m; the maximum collapsibility was around 1000 mm, and the length of the affected subway line was about 6 km. Simultaneously, the gushing water section of Xi'an Metro Line 4 was located in a busy urban area, and the underground pipeline was dense as well.

The water gushing occurred in a section of Xi'an Metro Line 4. The tunnel is located in the collapsible loess stratum, and scene investigation shows that the water rich in the tunnel site is weak. It is concluded that the groundwater is not developed, and the water content in the stratum is low. The site of water gushing disaster was initially discovered when the top of ring beam of segment appeared with a sudden water leakage in which the content continued to increase and accompanied by a large number of sediment emission. The assessment demonstrated that the water mainly derived from the water pipe (see Figure 1). Furthermore, the ground appeared subsidence, and the subsidence area was with the length, width, and depth of 20, 12, and 6.5 m, respectively.

2.2. Similar Materials. An experiment was carried out on the basis of water gushing from a tunnel in Xi'an Metro Line 4. Based on the actual engineering geological condition, it is assumed that the tunnel is completely located in the collapsible loess stratum in the model test, and the model test does

Table 1: Similarity ratios of physical quantities.

Physical quantity	Dimension	Similarity relation	Similarity ratio
l	L	$C_l = 25$	25
γ	$MT^{-2}L^{-2}$	$C_\gamma = 1$	1
σ	$MT^{-2}L^{-1}$	$C_\sigma = C_l C_\gamma$	25
ε	$M^0T^0L^0 = 1$	$C_\varepsilon = 1$	1
μ	$T^0M^0L^0 = 1$	$C_\mu = 1$	1
E	$MT^{-2}L^{-1}$	$C_E = C_\sigma$	25
k	$T^{-1}L$	$C_k = 1$	1
Q	$T^{-1}L^3$	$C_Q = C_k C_l^2$	625
u	$MT^{-2}L^{-1}$	$C_u = C_\sigma$	25
t	T	$C_t = \frac{C_l}{C_k}$	25
v	$T^{-1}L$	$C_v = C_k$	1

Table 2: Physical parameters of loess.

Parameter	Prototype	Model
Water content ω (%)	20	20
Bulk density γ (kN/m^3)	18.7	18.7
Void ratio e	0.757	0.757
Cohesion C (kPa)	30	30
Internal friction angle Φ (°)	20	20
Permeability coefficient k (m/d)	7	7
Elastic modulus E (kPa)	9.0×10^3	360
Poisson ratio μ	0.32	0.32

not take into account the influence of groundwater. The experimental testing has used dimensional analysis which is based on Buckingham's π theorem [56]. The theorem appropriately describes a relationship between physical variables and fundamental dimensions. It is pointed out that any physical equations can be transformed into equations of dimensionless quantities [57]. The model is a double-field coupled model under the combined action of stress field and seepage field [58–61]. The physical quantities to be considered in a stress field include geometrical dimension (l), bulk density (γ), stress (σ), strain (ε), Poisson's ratio (μ), and elastic modulus (E); the physical quantities to be considered in a seepage field include permeability coefficient (k), seepage velocity (v), seepage discharge (Q), and pore water pressure (u). All physical variables can be represented by fundamental dimensions which include time (T), quality (M), and length (L). The similarity ratios of various physical quantities are calculated, as shown in Table 1.

The actual parameters of loess are converted into theoretical similar parameters of the model according to similarity ratio, which is summarized in Table 2. According to the relevant literature and experimental results [27, 62–67], loess on the spot is used in this model test, and some barite powder, river sand, and industrial salt are added as surrounding rock materials. Barite powder can improve the cohesiveness of soil; river sand can improve the permeability of soil, and industrial salt can improve the collapsibility of soil. In the model test, bulk density is selected as the major controlling index. The elastic modulus of samples with different proportioning is measured by a universal press, and their internal friction angle and cohesive force are measured by direct shear tests. The test process and results of collapsibility of loess are shown in Figure 2. The proportioning basically meets the requirements of the model experiment. The proportioning of similar materials in the test is summed up in Table 3.

2.3. Model Equipment. The model test apparatus consists of three parts: test-bed, water injection control system, and measurement system. The test-bed is made of a tempered glass, and the sides are fixed with wooden boards. Its dimension is 1.5 m in length, 0.6 m in breadth, and 1.5 m in depth. Water injection control system includes a water storage system, water inlet pip, and pipe head. The pipe head was buried in the soil and connected with the inlet pipe. The other end of the inlet pipe was connected with a reservoir in which a water pump was placed there as well. The type of the water pump is YLJ-750; the pump head is 0 to 2 m, and the diameter of the water pipe is 16 mm, which accords with *China's Structural design code for pipelines of water supply and waste water engineering* (GB50332-2002). Sketch map of model test apparatus is shown in Figure 3. During the experiment, the measured physical quantities include pore water pressure, vertical stress of surrounding rock, and the strain of lining and surface settlement. Measurement of the lining strain used BE120-5AA type resistance strain gauge, and the data acquisition system employed JM3813 type static strain gauge. Measurement of the pore water pressure utilized YB-strain gauge. Measurement of the surface settlement used displacement meter. Measurement of the vertical stress of the surrounding rock employed pressure cell as well. The measuring device is shown in Figure 4.

2.4. Experiment Design and Procedures. In the experiment, four measurement sections are set up, including three longitudinal sections (denoted by A, B, and C) and one cross section (D). The measuring points of vertical stress of surrounding rock are arranged on the A, B, and C section. The measuring points of pore water pressure are arranged on the B and D sections. Since the experiment does not involve lining excavation, the strain measuring points are arranged along the circumferential direction of the lining. The measuring points of strain of lining are arranged on the A and B sections. The layout of each section and measuring point is shown in Figure 5. The measurement of surface settlement is arranged with 3 measuring lines, in which each measuring line has 4 measuring points (see Figure 6). The experiment procedure is shown in Figure 7.

2.5. Results and Analysis. In order to better analyze the real characteristics of water gushing, all the experimental data are converted to prototype by similarity ratio. From starting water injection to water gushing in the lining, experiment lasted for 4800 s. Experimental results showed that the tunnel

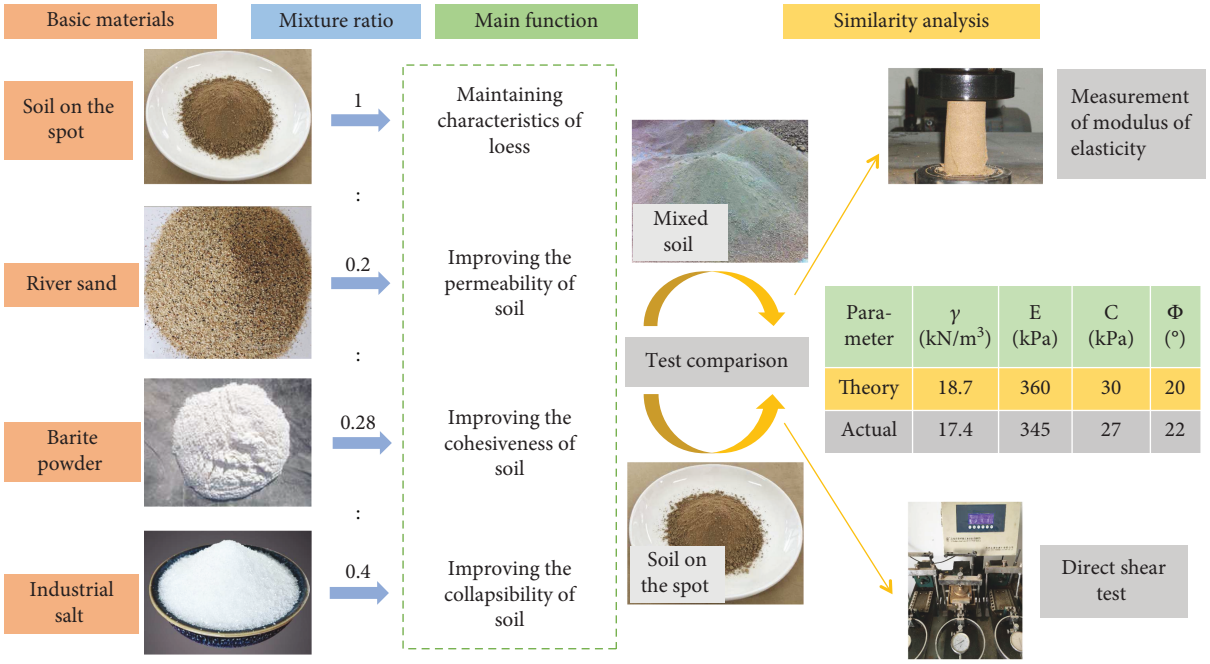

Figure 2: The test process and results of collapsibility of loess.

Table 3: The proportioning of similar material.

Structure	Proportioning
Surrounding rock	Soil on the spot : barite powder : river sand : industrial salt = 1 : 0.28 : 0.2 : 0.4
Lining	Water : barite powder : plaster = 1.7 : 0.1 : 1 Thickness: 120 mm; diameter: 250 mm

face appears to have water gushing, and a subsidence area with several cracks formed on the surface (see Figure 8). According to the data obtained during the experiment, the variation law of pore water pressure, vertical stress of surrounding rock, and the strain of lining and surface settlement were analyzed.

2.5.1. Pore Water Pressure. The time-history curve of pore water pressure of three measured points on the D section, as shown in Figure 9, demonstrated that the curves of the three measuring points are similar, and their numerical values are pretty close. From 100 to 2400 s, the pore water pressure of three points was gradually increasing, and the growth rate was faster. It illustrated that the water inflow channel in this direction was gradually formed and continued to expand. When the pore water pressure reached the peak, the water flowed along the channel to the circumference, and the pore water pressure of three points gradually decreased and tended to 0.

The time-history curve of pore water pressure of three measured points on the B section (see Figure 10) showed that the trends of the curves are approximately similar; however, the values of pore water pressure are different. S1 was located below the water gushing point, and from 100 to 3200, the pore water pressure of S1 gradually increased, and the growth rate was faster, while after 3600 s, the pore water pressure gradually tended to be stable. S2 was located at the 45 degrees' direction of the lining, and from 2400 to 3300 s, the pore water pressure of S2 gradually increased; however, after 3600 s, the pore water pressure gradually tended to be stable. The variation of the pore water pressure between S3 and S2 is similar; however, the pore water pressure of S3 is smaller than that of S2.

In conclusion, in the process of formation of water inflow channel, the main channel of water gushing is a channel beginning from the water gushing point to S1, while there is no large water inflow channel between S2 and S3. Three measuring points S4, S5, and S6 were located in the horizontal direction of the water gushing point, in which along these directions, the water gushing channel rapidly formed. However, with the formation of the main channel of water gushing, the water flow gradually decreased through these channels. The experimental results illustrated that the tunnel began to appear to have water gushing from the position of the arch crown of the tunnel face (see Figure 8(a)). It shows that the water will flow from the water source to the nearest surrounding of tunnel face, causing tunnel water gushing disaster.

2.5.2. Vertical Stress of the Surrounding Rock. Figure 11 represents the time-history curve of vertical stress of the surrounding rock of four measured points on the B section which was below the water gushing point. As depicted in Figure 11, the vertical stress variations of the three measuring points of Y4, Y5, and Y7 are similar. First, it was gradually increased, reached its peak value, and then gradually decreased after the period of stabilization. It reflected that the water inflow channel was smaller at the first and the stress of the surrounding rock gradually increased; however, with the continuous increasing of the water inflow, more water

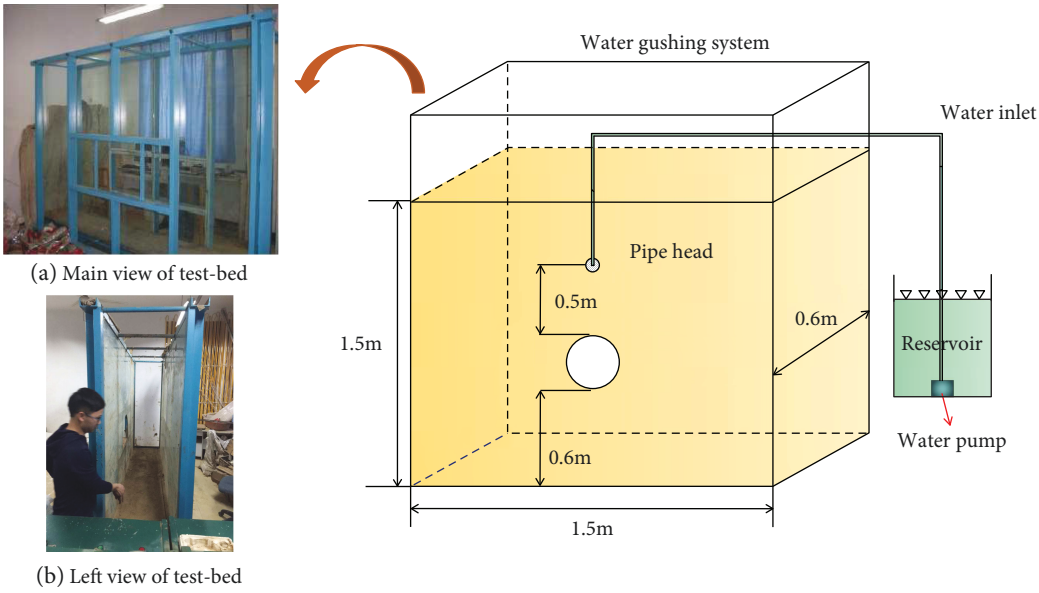

Figure 3: Sketch map of the model test apparatus.

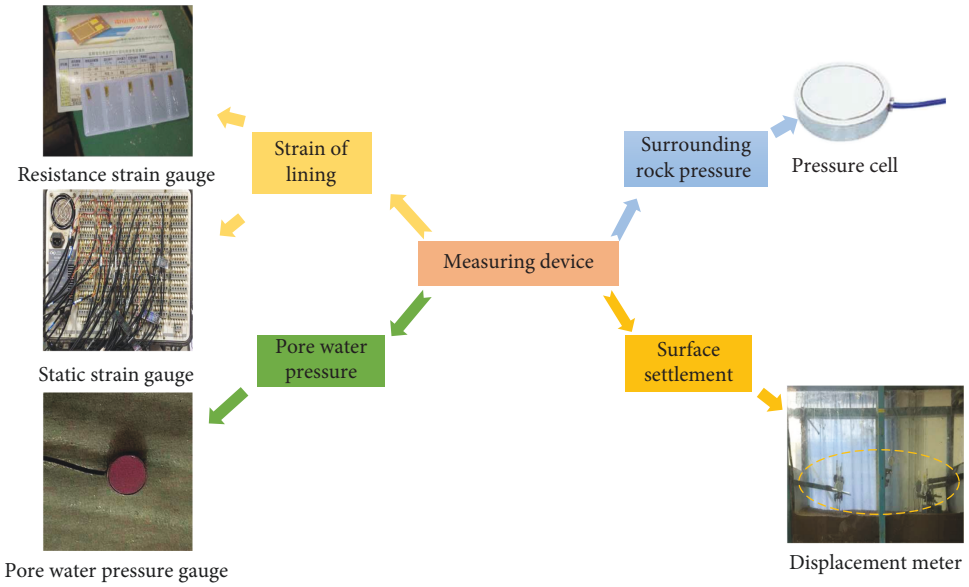

Figure 4: Measuring devices.

passages were formed, and the stress gradually decreased. The three differences are that the peak value of the stress of Y4 was the maximum; it rapidly decreased after the peak value, while the stress variation of Y7 gradually decreased after reaching the peak value and ran through the whole test process; the stress at the Y5 had a steady phase after the peak and then decreased gradually. It was indicated that the main channel of water gushing was the channel starting from the direction of Y4 to Y7, and it did not reach the tunnel bottom; the direction of Y4 to Y5 was the secondary channel.

Figure 12 shows the time-history curve of vertical stress of surrounding rock of three measured points on the A section, and Figure 13 displays the time-history curve of vertical stress of the surrounding rock of three measured points on the C section. It can be seen that the variation of the surrounding rock of three measuring points on the A and C sections are similar to the variation of Y4, Y5, and Y6 on the B section; however, their stress values are smaller. It was indicated that the direction of Y1 to Y3 and the direction of Y8 to Y10 were the secondary channels of water gushing, while they did not reach at the bottom of the tunnel; the direction of Y1 to Y2 and the direction of Y8 to Y9 were permeable channels, which had trivial impact on the surrounding rock.

According to the formation of the mentioned water gushing channels, it can be concluded that in the experimental model, the range of water gushing was within 20 cm around the water gushing point and 50 cm below the water gushing point. In addition, it can be concluded that the stress

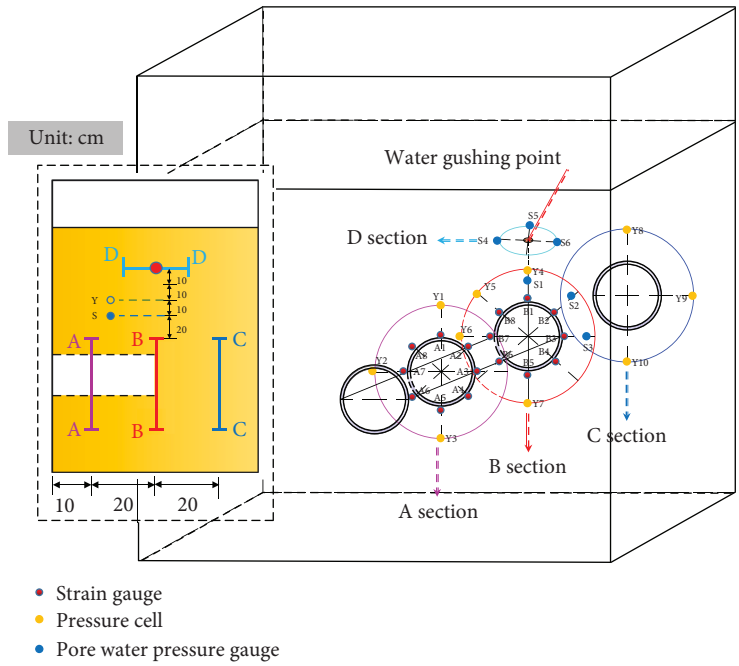

Figure 5: Monitoring section and measuring points' layout.

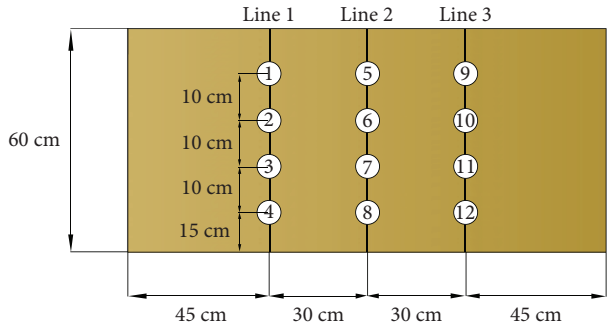

Figure 6: Layout of monitoring points for surface settlement.

distribution of the surrounding rock gradually decreased from the arch crown to the two sides when the water gushing point is located above the lining. The reason may be attributed to the mechanical properties of the soil above the arch crown, which were changed due to the combination of soil and water. When the loess encountered with water, its collapsibility gradually revealed, its fluidity enhanced, and the stress of the surrounding rock above the tunnel gradually increased. With the increasing of water content, the water flow caused the soil to move to the four sides, which aggravated the soil erosion and led to gradually increase the stress of the surrounding rock on both sides of the lining. When the water gushing channels gradually formed and the water flow was dispersed and formed more channels, the vertical stress of the surrounding rock gradually decreased. Moreover, based on the results of the experiment, it can be seen that the surrounding rock above the tunnel collapsed, so it can be inferred that the arching effect of the surrounding rock above the lining vault is lost due to soil erosion, resulting in surface subsidence.

2.5.3. The Strain of the Lining. Figure 14 depicts the time-history curve of the strain of the lining for eight measured points on the A section, and Figure 15 is the time-history curve of the strain of lining for eight measured points on the C section. As shown in Figure 14, the strain of the lining of the eight points on the A section slightly varied before 4000 s, in which after 4000 s, it notably changed. Among them, the stresses of A1, A2, A5, and A6 were positive (tensile stresses), and from 4000 to 4300 s, they gradually increased, in which the growth rate was faster, and they gradually stabilized after 4300 s. Additionally, the stresses of A3, A4, A7, and A8 were negative (compressive stresses), and from 4000 to 4300 s, they gradually increased, in which the growth rate was faster and gradually stabilized after 4300 s. It can be seen from Figure 15 that the strain variation of the measurement points on the B section was basically the same as that of the A section.

It has been indicated that the lining in the longitudinal direction made tensile deformation, and both sides of the lining made inward contraction; the overall stress of the lining is "peanut shell" shape. When gushing water formed a main water channel with vertical direction and an auxiliary water channel with horizontal direction, the soil above the tunnel was squeezed to the sides of the lining, resulting in the deformation of the lining. Since the lining had a certain distance from the water source, the stress of the lining gradually increased, which occurred in the second half of the experiment. This is consistent with the conclusions drawn from the vertical stress of the surrounding rock.

2.5.4. Surface Settlement. Figure 16 displays the surface subsidence curve of three measuring lines. It can be seen that the settlement values of the three measuring lines increased with the increase of axis distance, in which among them, the

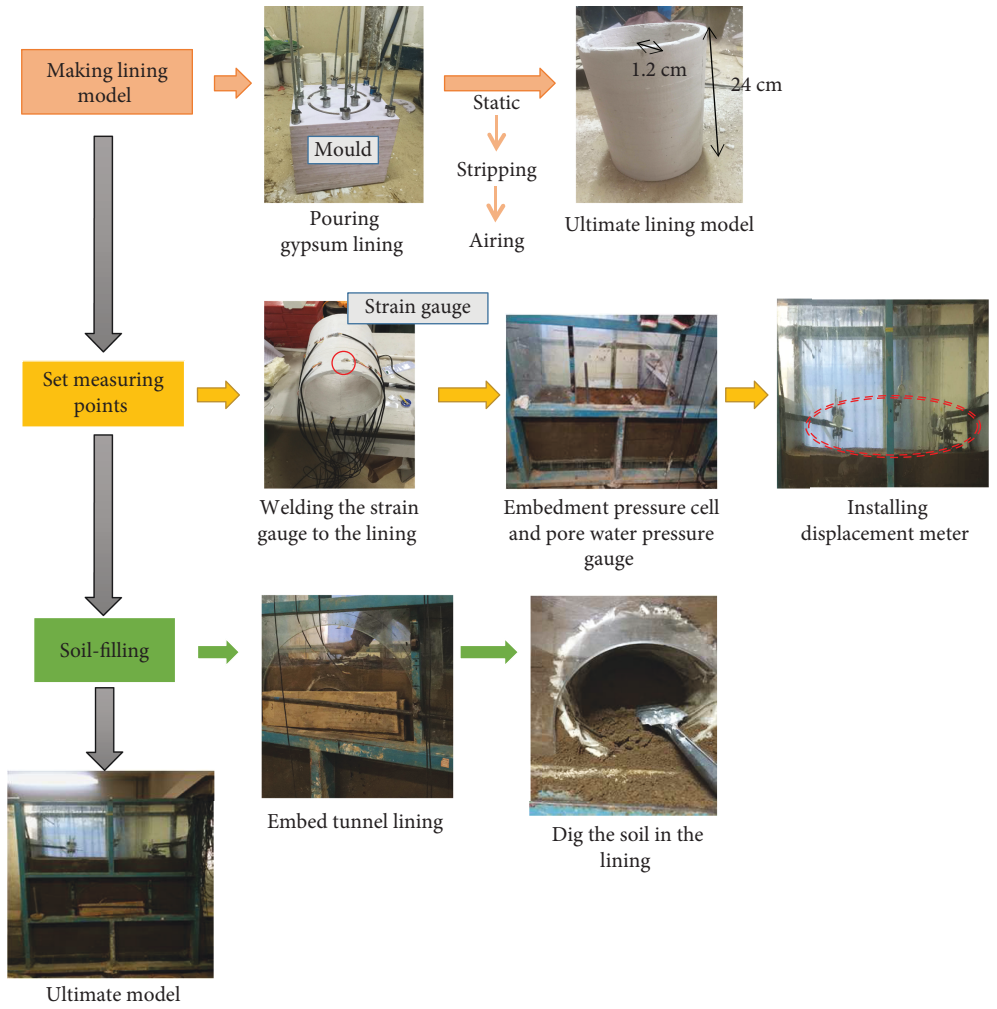

Figure 7: Experiment procedure.

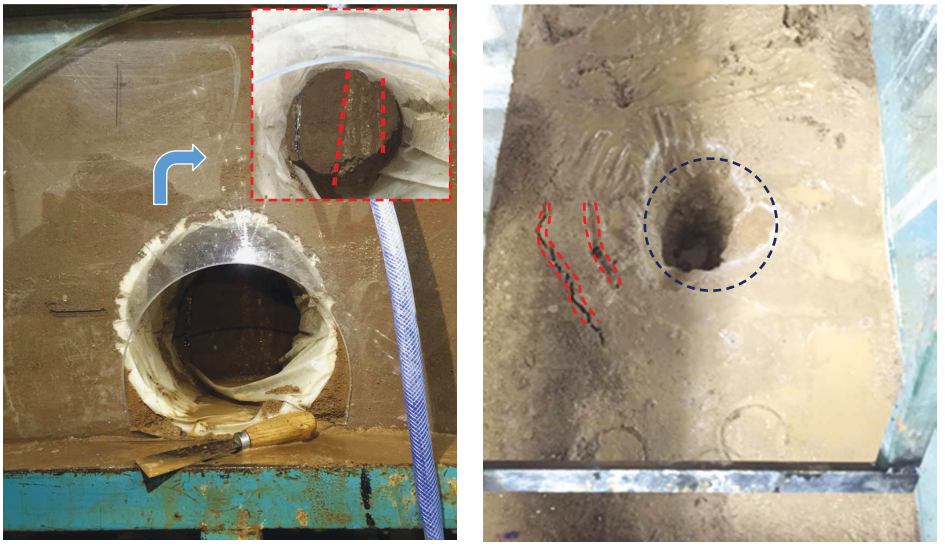

(a) (b)

Figure 8: Experiment results. (a) Water gushing in lining; (b) subsidence area.

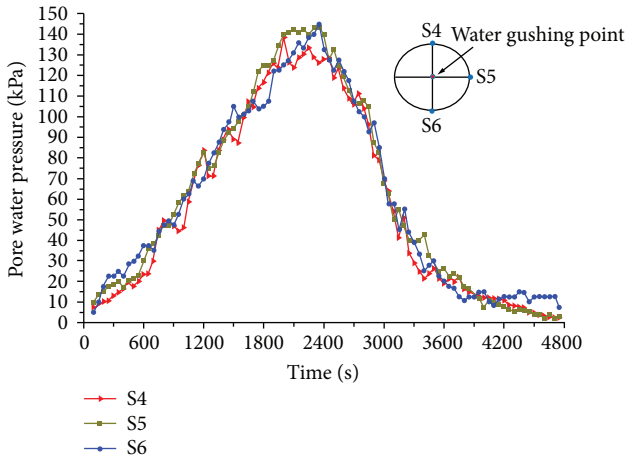

Figure 9: Pore water pressure–time curves of S4, S5, and S6.

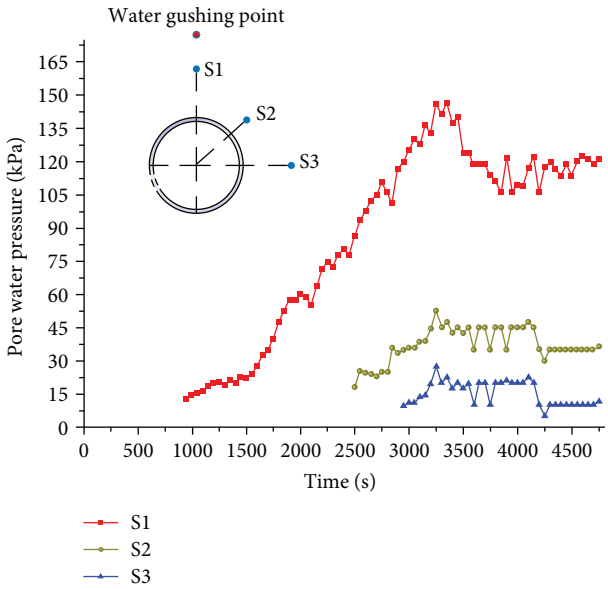

Figure 10: Pore water pressure–time curves of S1, S2, and S3.

settlement values of lines 1 and 3 were smaller, while the settlement value of line 2 was larger, indicating that the main water gushing channel was along the direction of line 2, and there were no main water gushing channels in the soil layers of lines 1 and 3. This is because the measuring line 2 was located above the tunnel, in which during the process of water gushing, the tunnel would not significantly deform due to the action of water flow. However, the surrounding soil would settle; thus, the farther distance from the tunnel lining, the greater settlement of the soil layer.

3. Modeling Analysis

The main objective of this study is investigating the characteristic of gushing water near the tunnel face, which the influence of tunnel excavation is not considered. In the modeling process, in order to highlight the main objective, the problem is simplified as a plane strain problem. Therefore, a two-dimensional tunnel water-inflow model was developed using

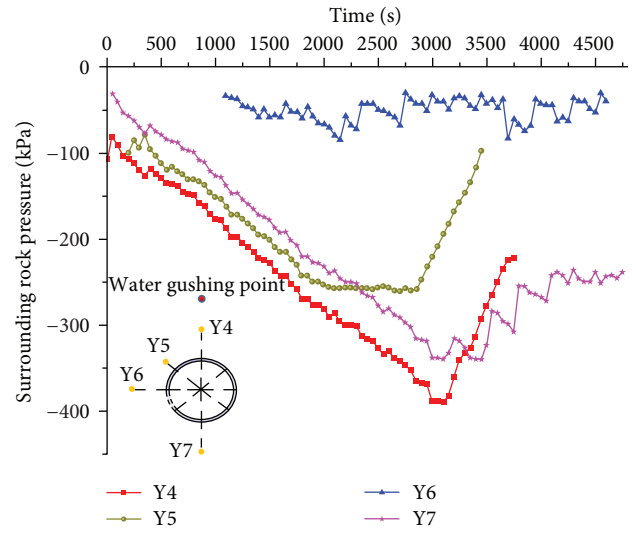

Figure 11: Surrounding rock pressure–time curves of Y4, Y5, Y6, and Y7.

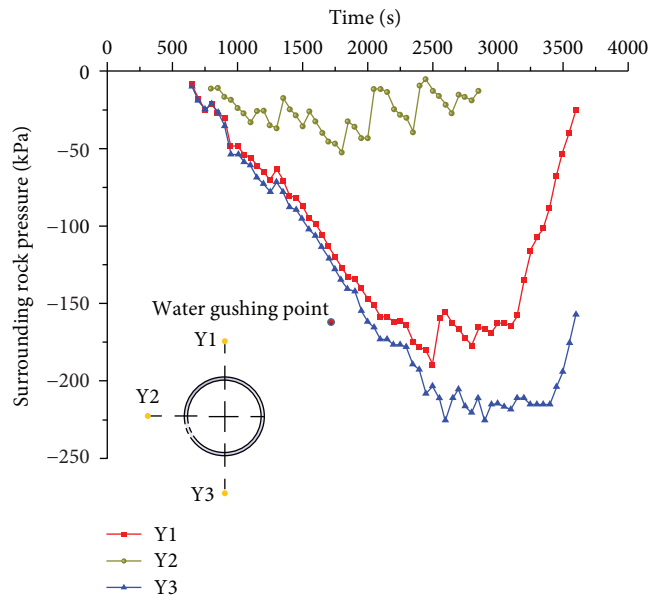

Figure 12: Surrounding rock pressure–time curves of Y1, Y2, and Y3.

the ABAQUS [68] finite element software to simulate the flow state of water flow in a saturated loess layer.

3.1. Modeling Introduction. Module of coupling of seepage and stress in the ABAQUS was used for analysis. In the modeling process, the porous loess layer was regarded as multiphase materials, and the unit type was four-node plane strain element (CPE4). The lining was regarded as an elastic element, and the stiffness of element was calculated according to the elastic modulus and Poisson's ratio of the steel and concrete. Model of seepage and stress coupling, which is based on large deformation of clay, was developed by using the updated Lagrangian method. The soil model followed the Mohr-Coulomb failure criterion [69], and the pore water pressure obeyed Darcy's law in order to appropriately

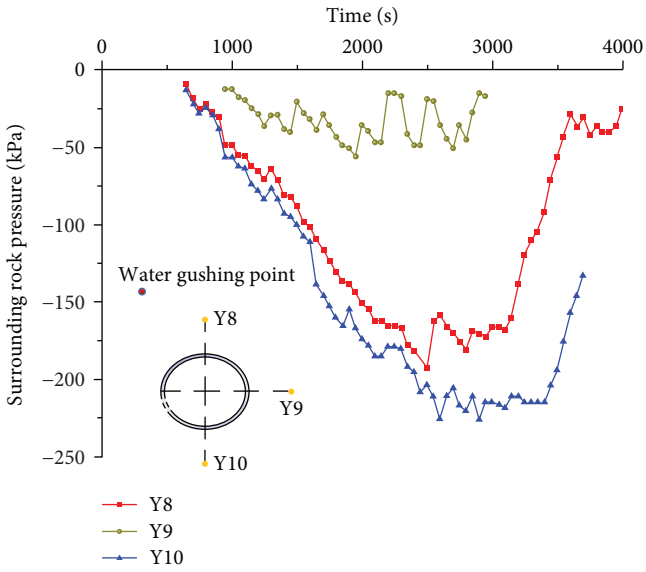

Figure 13: Surrounding rock pressure–time curves of Y8, Y9, and Y10.

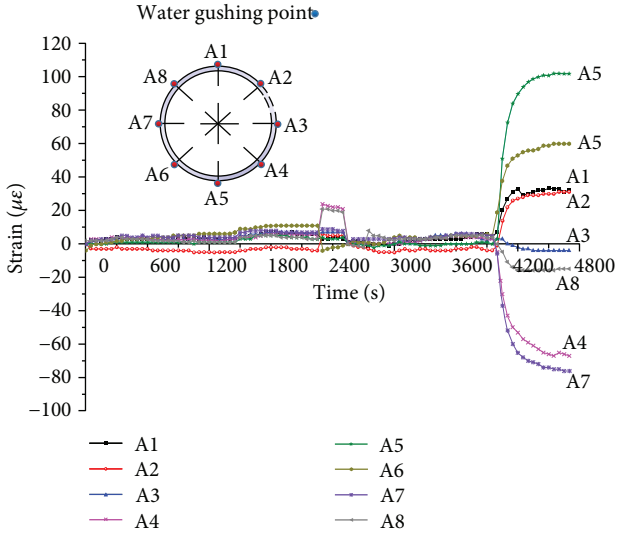

Figure 14: Strain-time curves of A1–A8 on the A section.

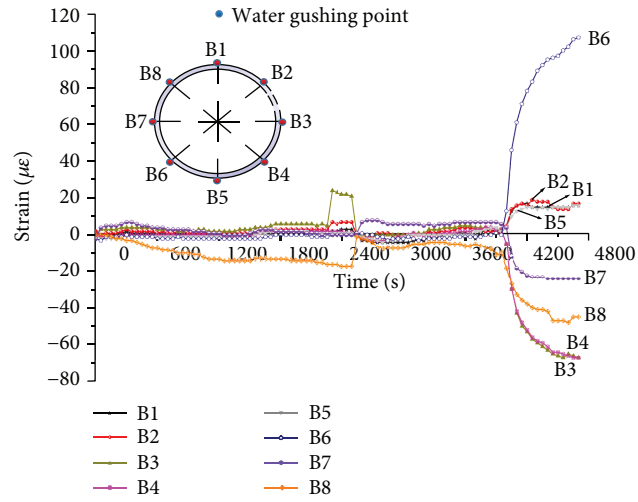

Figure 15: Strain-time curves of B1–B8 on the B section.

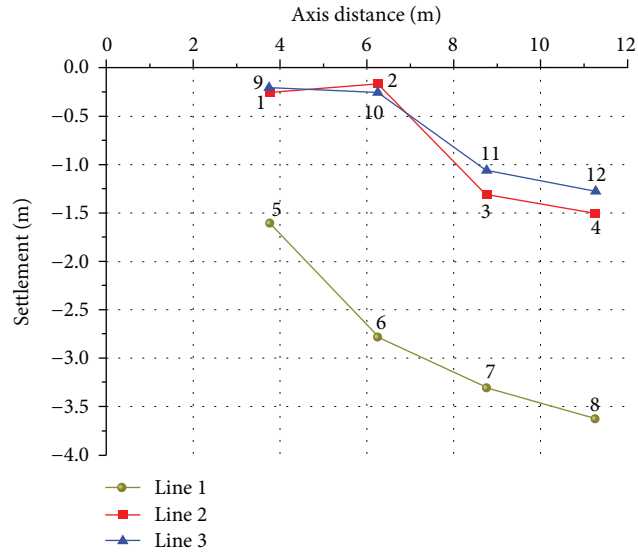

Figure 16: Surface subsidence curve.

simulate the seepage of saturated loess. In the modeling, the lower boundary of the model restricted displacement in the X and Y directions, in which two sides of the model restricted displacement in the X direction. Applying the corresponding node pore pressure function to the node of the pipe to simulate the water out state of the pipeline, the boundary pore pressure under the stratum was set to 0, and using the pressure head and gravity action, the water seepage in the soil layer was realized. In the computation, the analysis of the stability of crustal stress was initially performed, and then, the transient analysis of fluid-structure interaction was conducted. In the process of transient analysis, the pipe outlet time was set to 3600 s. The model consists of 6 operating conditions, as listed in Table 4. The Saint Venant principle showed that the model size is generally 3~5 times of the hole diameter, in which due to the limitations of the test box, the boundary of the test model was not fully selected according to the actual size. However, in numerical modeling, in order to more accurately simulate the actual situation, the size of the model was taken into account as length of 50 m, width of 50 m, the lining diameter was 6 m, and thickness and burial depth of tunnel were 30 cm and 15 m, respectively, as shown in Figure 17. The physical and mechanical properties of the lining are listed in Table 5 as well.

3.2. Analysis of Calculation Results

3.2.1. Comparison and Analysis of Working Condition 1 and Model Experiment. The simulation process of operating condition 1 is similar to the experimental model. The measurement points in the same positions of the B section, as shown in Figure 5, are selected in the finite element modeling, and the variation of the relevant results with the time was analyzed in order to verify the correctness of the law obtaining based on experimental model.

Table 4: Model operating condition.

Operating condition	Effluent point	Water pressure (MPa)	Lining patterns
Condition 1	1	0.25 MPa	Segment lining
Condition 2	2	0.25 MPa	Segment lining
Condition 3	3	0.25 MPa	Segment lining
Condition 4	1	0.2 MPa	Segment lining
Condition 5	1	0.15 MPa	Segment lining
Condition 6	1	0.25 MPa	Composite lining

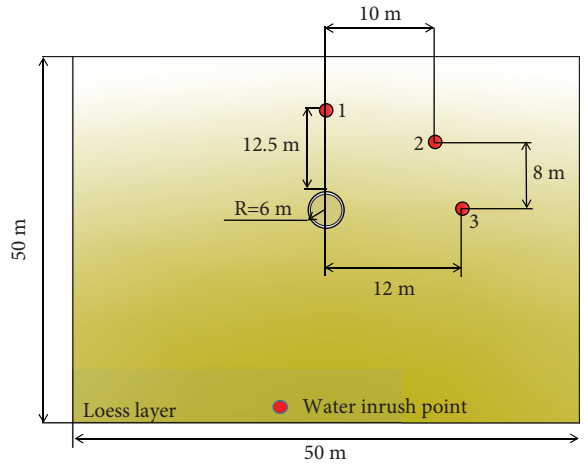

Figure 17: Model schematic diagram.

(1) Pore Water Pressure. The law of pore water pressure regarding the variation of three points computed by finite element analysis is depicted in Figure 18. The analysis results showed that the pore water pressure of the three points gradually increased with the passing of time and gradually decreased at within 1500s. This law is partially consistent with the law derived from the experimental model, and the reason for the difference is that the process simulated by the finite element method was longer than the experimental model. When the flow time was longer, more loess would contact with the water flow, which would lead to the reduction of water flow in the same location, and the pore water pressure around the lining was gradually decreased.

Figure 19 displays the path of water flow in different time periods for condition 1, and the blue region indicates the affected area of the water flow. It can be seen that when the direction of effluent was not limited, under the dual actions of water pressure and gravity, the water would mainly flow in the direction of gravity and then formed the flow channel. The position of 1 to 2 m, based on the ground surface, was the highest position of the flow upward, indicating that the soil layer at this height would be affected by water gushing. In addition, the soil layer within the double diameter ranges of the left and right sides of the tunnel was affected by water gushing. A well agreement between the results of finite element analysis and experimental was observed as well.

(2) Vertical Stress of the Surrounding Rock. In ABAQUS, the tensile stress is defined as positive, and the compressive stress

Table 5: Physical and mechanical properties of the lining.

Parameter	Bulk density γ (kN/m^3)	Elastic modulus E (kPa)	Poisson ratio μ	Thickness h (m)
Lining	24	3.45×10^7	0.3	0.3

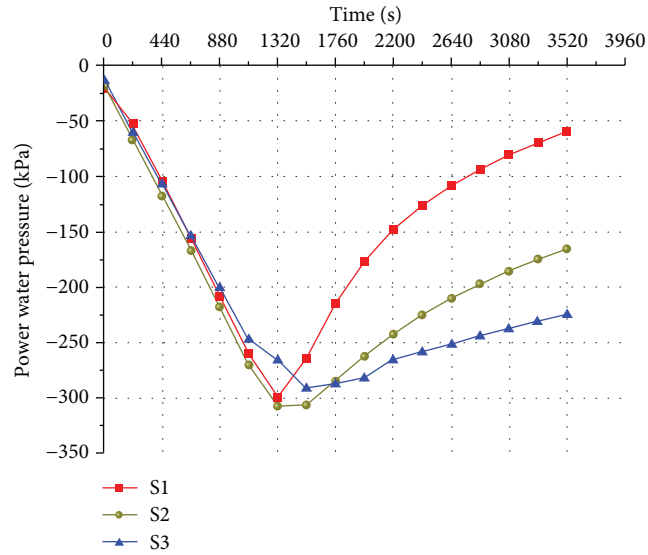

Figure 18: Pore water pressure–time curves of S1, S2, and S3.

is negative. As shown in Figure 20, the vertical stress of the four points gradually increased with time and then gradually decreased after reaching its peak. This is basically the same in the experimental model, and the difference is described by the curve of Y6. In the experimental model, the vertical stress value of Y6 was very small, and the amplitude of the variation was not very much, while in the finite element analysis, the vertical stress of Y6 was great. This may be attributed to a fact that in the experimental model, the water flow had not been affected by the soil layer at the top of Y6. However, in the finite element analysis, the water pressure was closer to the actual situation, and the water flow formed a passage around the lining as well.

(3) The Stress of the Lining. The cloud picture of the maximum principal stress of the lining is shown in Figure 21. It can be seen that the two sides of the lining were compressed and the top and the bottom were drawn. This is in agreement with analyzing the experimental model. Figure 22 shows the time-history curve of the stress for lining. As illustrated in Figure 21, B1 at the vault and B5 at the bottom, the stress variation was initially increased and then decreased; the stress of B3 was gradually increased, while the stresses of B2 and B4 were slightly changed. It can be concluded that when the tunnel produced water gushing, the top and both sides of the lining are the main force zones, requiring to be considered in the process of monitoring.

(4) Surface Settlement. Selecting 5 measuring points in the range of 10 m on the right side of the ground surface above the center line of the tunnel, the distance between each measuring point is 2 m; point 1 was the closest to the center line,

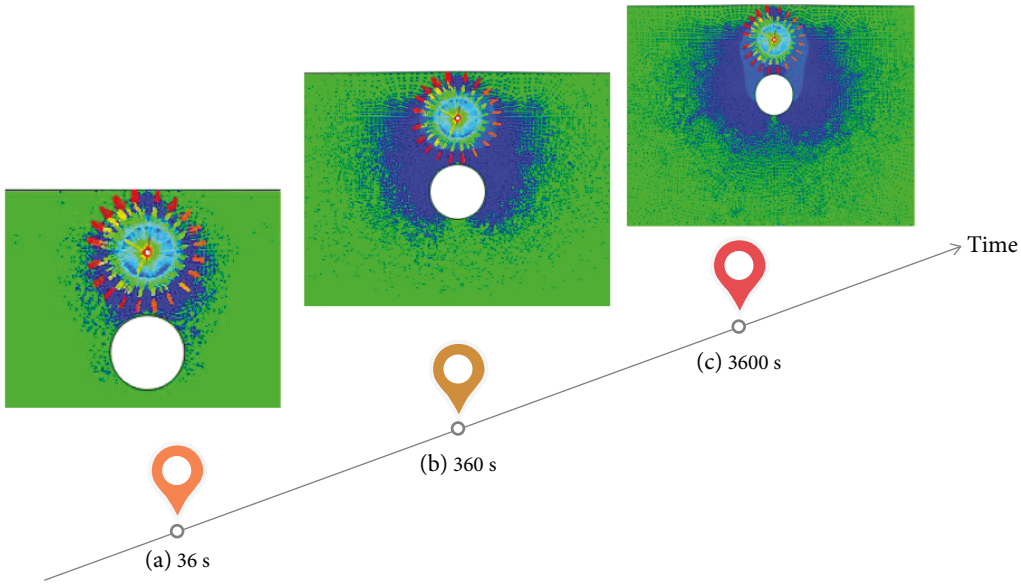

Figure 19: The path of water flow in a different time period of condition 1.

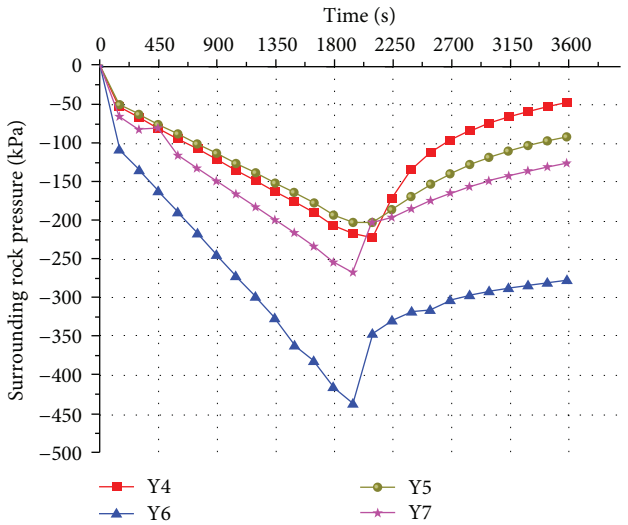

Figure 20: Surrounding rock pressure–time curves of Y4, Y5, Y6, and Y7.

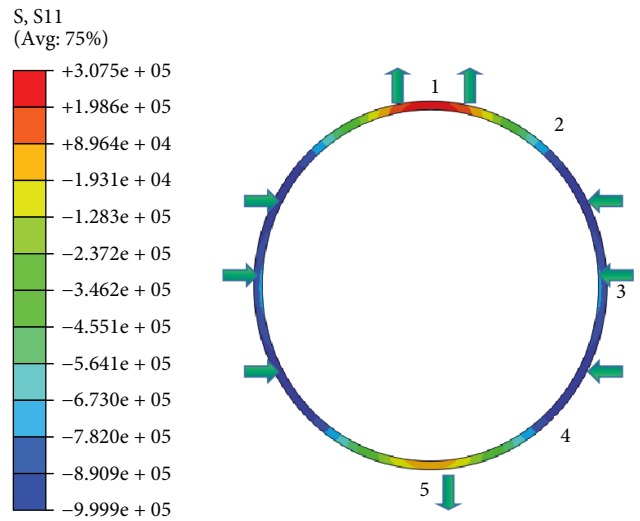

Figure 21: The cloud picture of the maximum principal stress of the lining (Pa).

while point 5 was the farthest from the center line (see Figure 23). Figure 23 displays the surface subsidence curve of the five measuring points. It can be seen that the closer to the water gushing point, the greater the settlement of the soil layer, which is in agreement with the results of the experimental model.

In summary, the experimental findings were verified by numerical simulation. Combined with other operating conditions, the flow state of water in different water pressures, along with different water gushing points, and various types of tunnel lining in saturated loess stratum should be further analyzed in order to study the pore water pressure field of the surrounding rock, the force condition of the lining, and the distribution law of the displacement of the stratum.

3.2.2. Distribution of Pore Water Pressure Field in the Surrounding Rock. Figure 24 shows the path of the water flow for four different conditions under the same time and water pressure. As illustrated in Figures 24(a)–24(c), there is a significant variation in the flow path of the water when the water outlet position is different. When the outlet position was above the lining, under the dual actions of water pressure and gravity, a vertical main flow channel was formed, while the top and both sides of the lining were the main areas of water flow; when the outlet point was located in the 45 degrees' direction of the lining, a 45-degree flow channel was formed, which the main areas of water flow were the top of the lining and a side near the water outlet point, and there was no apparent water channel within 5 m below the surface. When the outlet point was in the horizontal

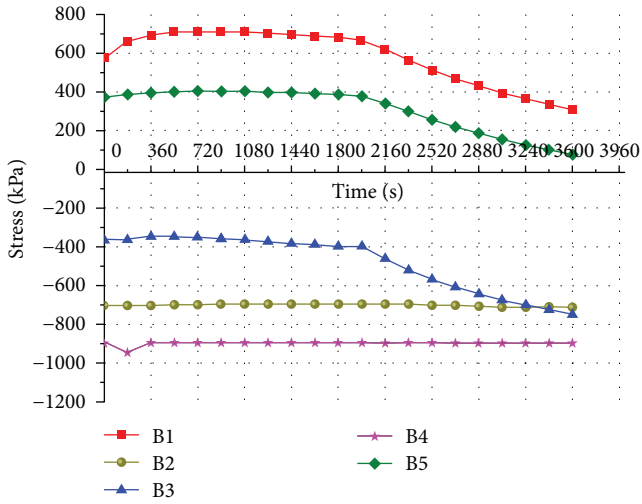

Figure 22: Stress-time curves of B1–B5.

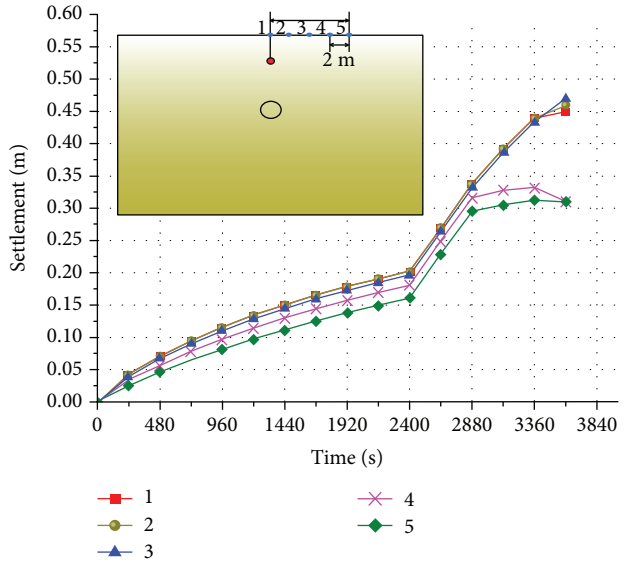

Figure 23: Surface subsidence curve.

direction of the lining, the water would still flow to the surrounding of the lining due to the action of water pressure, and the arch bottom and the side near the water outlet point were the main areas of water flow. As shown in Figure 24(a), the flow channels are roughly the same, while there is a difference in the areas of water flow. When the type was composite lining, the flow of water was more uniform around the lining, and when the type was segment lining, the flow of water was less in the part of the arch bottom.

3.2.3. Distribution of Stress Field of the Lining. Figure 25 illustrates the cloud picture of the maximum principal stress of the lining for four different conditions in various water pressures and different forms of lining. As displayed in Figures 25(a)–25(c), with decreasing the water pressure of the outlet point, the tensile stress of the top and bottom of the lining was increased, while the compressive stress on both sides decreased, indicating that during the same time, the greater the water pressure was, the more complete water flow channel was formed; consequently, more surrounding rocks were moved to both sides of the lining, resulting in the increase of compressive stress on both sides of the lining. As shown in Figures 25(a) and 25(d), the composite lining was fully pressed, which was different from the force of segment lining, indicating that when the soil layer produces gushing water, the whole composite lining is mainly compressed, in which the stress on both sides of the arch foot and shoulder part is the largest.

3.2.4. Distribution of Displacement Field of the Surrounding Rock. Under the same time and outlet location, the effect of different water pressures on the settlement of the stratum is basically the same, and the only difference is related to the settlement value. Figure 26 shows surface subsidence under different water pressures. As depicted in Figure 26, when the water pressure is 0.25 MPa, the maximum settlement is 0.48 m; when the water pressure is 0.20 MPa, the maximum settlement is 0.44 m; when the water pressure is 0.15 MPa, the maximum settlement is 0.41 m. It is concluded that the water pressure directly affects the surface subsidence, the larger the water pressure, the greater surface settlement is obtained.

4. Conclusions

Based on the water gushing disaster of a section tunnel on Xi'an Metro Line 4, the structural response and damage evolution of the tunnel in loess region under local hydrodynamic environment are systematically studied by model test and numerical simulation. The main conclusions:

(1) The experimental model and the numerical simulation in the condition 1 verified each other. When the water outlet point is above the lining, the stress distribution of the surrounding rock is gradually reduced from the arch crown to both sides, and the overall stress of the lining is "peanut shell"; the gushing water forms a main water channel with vertical direction and an auxiliary water channel with horizontal direction. In the process of water gushing, the closer to the water source, the greater pore water pressure is; the closer to the water source, the greater surface subsidence is, while in the direction of the tunnel axis, the settlement of the stratum which has the lining is smaller than that of the stratum without lining

(2) When the position of the water outlet changes, the channel form of the flow to the lining is also varied; when the outlet point is located in the 45 degrees' direction of the lining, a 45-degree flow channel is formed. In addition, when the outlet point is in the horizontal direction of the lining, the main channel of the water flow does not pass through the lining; however, there will be a small amount of water flowing into the lining near the water outlet point. Under the same water outlet position, the flow of water

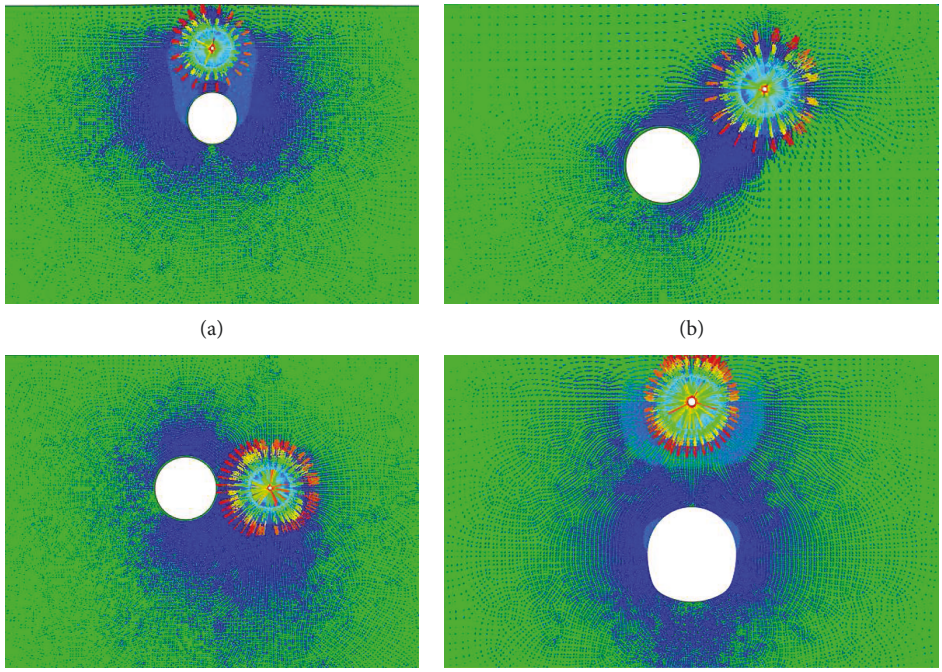

Figure 24: The path of the water flow of four conditions. (a) Condition 1; (b) condition 2; (c) condition 3; and (d) condition 6.

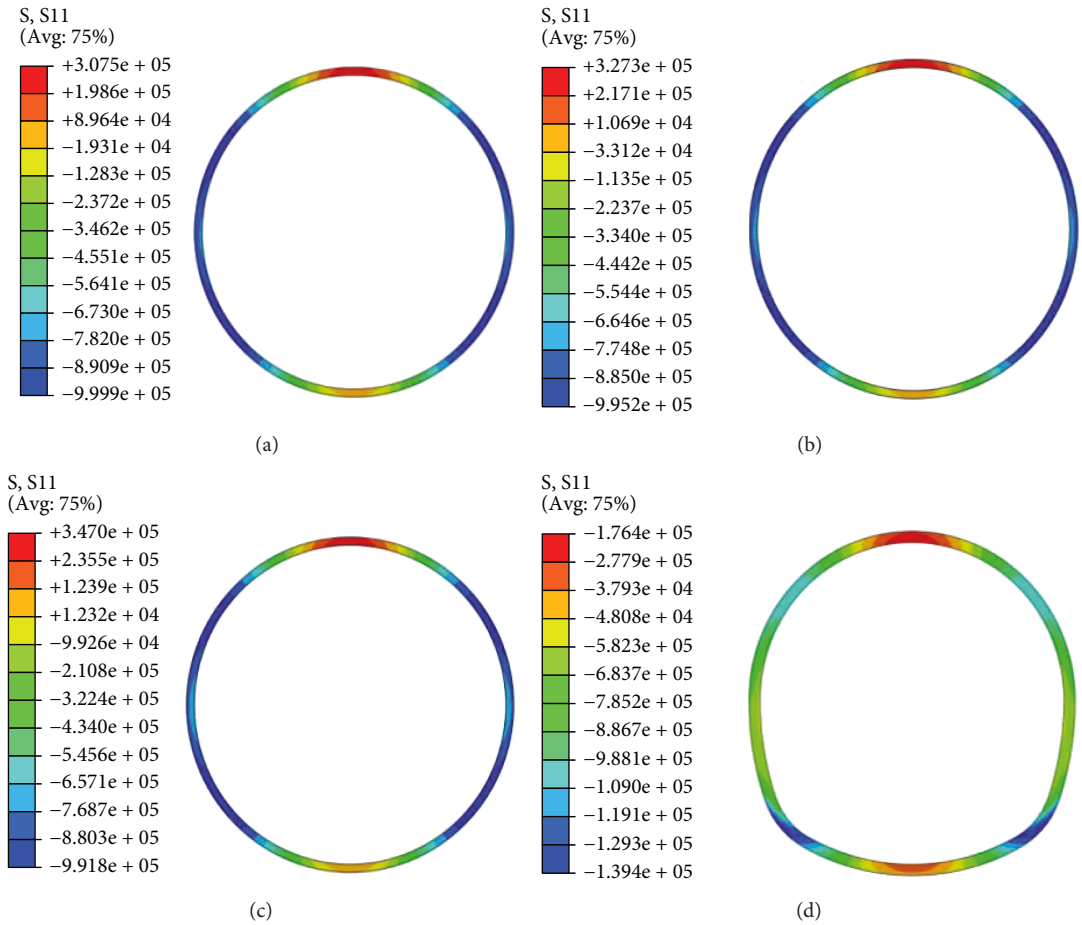

Figure 25: The maximum principal stress of the lining of four conditions (unit: Pa). (a) Condition 1; (b) condition 4; (c) condition 5; and (d) condition 6.

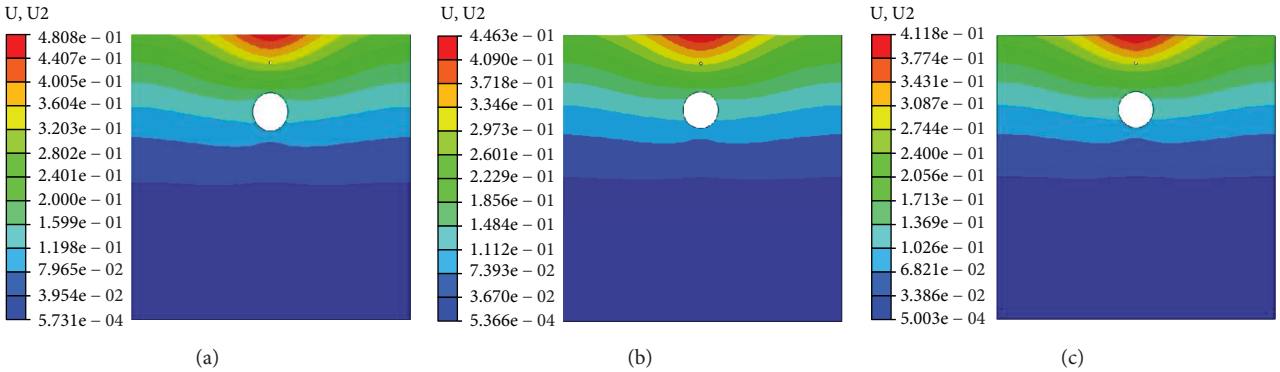

Figure 26: Surface subsidence under different water pressure (unit: m). (a) Condition 1; (b) condition 4; and (c) condition 5.

around composite lining is more uniform, while there is less flow at the bottom of segment lining

(3) As the water pressure of the outlet point decreases, the tensile stress of the top and bottom of the lining increases, while the compressive stress on both sides decreases; segment lining is subjected to pressure on both sides and the vault and arch bottom are pulled, while composite lining is mainly subjected to compression, and the compressive stress at both ends of the arch foot is the largest

(4) The water pressure directly affects the surface subsidence; the larger the water pressure, the greater surface settlement is; however, the settlement range is mainly affected by time, that is, the longer the time of water gushing, the greater scope of the surface subsidence is obtained

Data Availability

The data used to support the findings of this study are available from the corresponding author upon request.

Conflicts of Interest

The authors declare that there is no conflict of interests regarding the publication of this paper.

Acknowledgments

This work is financially supported by the National Key R&D Program of China (no. 2018YFC0808706) and the Project on Social Development of Shaanxi Provincial Science and Technology Department (nos. 2018SF-382, 2016SF-412).

References

[1] J. O. Snowden, R. R. Priddy, and C. D. Caplenor, *Loess Investigations in Mississippi: Geology of Mississippi Loess*, Mississippi Geological, Economic and Topographical Survey, 1968.

[2] G. Gao, "The distribution and geotechnical properties of loess soils, lateritic soils and clayey soils in China," *Engineering Geology*, vol. 42, no. 1, pp. 95–104, 1996.

[3] Q. Liang, J. Li, X. Wu, and A. Zhou, "Anisotropy of Q_2 loess in the Baijiapo Tunnel on the Lanyu Railway, China," *Bulletin of Engineering Geology and the Environment*, vol. 75, no. 1, pp. 109–124, 2016.

[4] M. Zhang and J. Liu, "Controlling factors of loess landslides in western China," *Environmental Earth Sciences*, vol. 59, no. 8, pp. 1671–1680, 2010.

[5] Q. Wang and H. Sun, "Traffic structure optimization in historic districts based on green transportation and sustainable development concept," *Advances in Civil Engineering*, vol. 2019, Article ID 9196263, 15 pages, 2019.

[6] P. Li, F. Wang, and Q. Fang, "Undrained analysis of ground reaction curves for deep tunnels in saturated ground considering the effect of ground reinforcement," *Tunnelling and Underground Space Technology*, vol. 71, pp. 579–590, 2018.

[7] T. X. Zhu, "Gully and tunnel erosion in the hilly Loess Plateau region, China," *Geomorphology*, vol. 153-154, pp. 144–155, 2012.

[8] Y. Bai, Z. Dai, and W. Zhu, "Multiphase risk-management method and its application in tunnel engineering," *Natural Hazards Review*, vol. 15, no. 2, pp. 140–149, 2014.

[9] S. Rezaeimalek, A. Nasouri, J. Huang, S. Bin-Shafique, and S. T. Gilazghi, "Comparison of short-term and long-term performances for polymer-stabilized sand and clay," *Journal of Traffic and Transportation Engineering (English Edition)*, vol. 4, no. 2, pp. 145–155, 2017.

[10] R. Qiao, Z. Shao, W. Wei, and Y. Zhang, "Theoretical Investigation into the Thermo-Mechanical Behaviours of Tunnel Lining During RABT Fire Development," *Arabian Journal for Science and Engineering*, 2018, in press.

[11] C. Liu, Z. Fan, X. Chen, C. Zhu, and G. Bai, "Experimental study on bond behavior between section steel and RAC under full replacement ratio," *KSCE Journal of Civil Engineering*, vol. 23, no. 2, pp. 1–12, 2019.

[12] Z.-F. Wang, W.-C. Cheng, and Y.-Q. Wang, "Investigation into geohazards during urbanization process of Xi'an, China," *Natural Hazards*, vol. 92, no. 3, pp. 1937–1953, 2018.

[13] X. Pang, J. Singh, and W. Cuello Jimenez, "Characterizing gas bubble size distribution of laboratory foamed cement using X-ray micro-CT," *Construction and Building Materials*, vol. 167, pp. 243–252, 2018.

[14] J. Lai, K. Wang, J. Qiu, F. Niu, J. Wang, and J. Chen, "Vibration response characteristics of the cross tunnel structure," *Shock and Vibration*, vol. 2016, Article ID 9524206, 16 pages, 2016.

[15] Y. Wei, S. Liang, W. Guo, and W. Hansen, "Stress prediction in very early-age concrete subject to restraint under varying

temperature histories," *Cement and Concrete Composites*, vol. 83, pp. 45–56, 2017.

[16] P. F. Li, F. Wang, L. F. Fan, H. D. Wang, and G. W. Ma, "Analytical scrutiny of loosening pressure on deep twin-tunnels in rock formations," *Tunnelling and Underground Space Technology*, vol. 83, pp. 373–380, 2019.

[17] J. Wang, Q. Huo, Z. Song, and Y. Zhang, "Study on adaptability of primary support arch cover method for large-span embedded tunnels in the upper-soft lower-hard stratum," *Advances in Mechanical Engineering*, vol. 11, no. 1, pp. 1–15, 2019, in press.

[18] Y. Luo, J. Chen, P. Huang, M. Tang, X. Qiao, and Q. Liu, "Deformation and mechanical model of temporary support sidewall in tunnel cutting partial section," *Tunnelling and Underground Space Technology*, vol. 61, pp. 40–49, 2017.

[19] Z. Wang, Y. Xie, and H. Liu, "Analysis on deformation and structural safety of a novel concrete-filled steel tube support system in loess tunnel," *European Journal of Environmental and Civil Engineering*, 2018, in press.

[20] H. Yu, Y. Yuan, G. Xu, Q. Su, X. Yan, and C. Li, "Multi-point shaking table test for long tunnels subjected to non-uniform seismic loadings - Part II: application to the HZM immersed tunnel," *Soil Dynamics and Earthquake Engineering*, vol. 108, pp. 187–195, 2018.

[21] Q. Yan, H. Chen, W. Chen, J. Zhang, S. Ma, and X. Huang, "Dynamic characteristic and fatigue accumulative damage of a cross shield tunnel structure under vibration load," *Shock and Vibration*, vol. 2018, Article ID 9525680, 14 pages, 2018.

[22] Q. Yan, W. Zhang, C. Zhang, H. Chen, Y. Dai, and H. Zhou, "Back Analysis of Water and Earth Loads on Shield Tunnel and Structure Ultimate Limit State Assessment: A Case Study," *Arabian Journal for Science and Engineering*, 2018, in press.

[23] Z.-F. Wang, S.-L. Shen, W.-C. Cheng, and Y.-S. Xu, "Ground fissures in Xi'an and measures to prevent damage to the Metro tunnel system due to geohazards," *Environmental Earth Sciences*, vol. 75, no. 6, p. 511, 2016.

[24] S. He, L. Su, H. Fan, and R. Ren, "Methane Explosion Accidents of Tunnels in SW China," *Geomatics, Natural Hazards and Risk*, vol. 10, no. 1, pp. 1–15, 2019, in press.

[25] Y. Fang, J. Guo, J. Grasmick, and M. Mooney, "The effect of external water pressure on the liner behavior of large cross-section tunnels," *Tunnelling and Underground Space Technology*, vol. 60, pp. 80–95, 2016.

[26] Y. Fang, C. He, A. Nazem, Z. Yao, and J. Grasmick, "Surface settlement prediction for EPB shield tunneling in sandy ground," *KSCE Journal of Civil Engineering*, vol. 21, no. 7, pp. 2908–2918, 2017.

[27] R. Ren, H. Zhou, Z. Hu, S. He, and X. Wang, "Statistical Analysis of Fire Accidents in Chinese Highway Tunnels 2000-2016," *Tunnelling and Underground Space Technology*, vol. 83, pp. 452–460, 2019.

[28] L. Tong, L. Liu, G. Cai, and G. du, "Assessing the coefficient of the earth pressure at rest from shear wave velocity and electrical resistivity measurements," *Engineering Geology*, vol. 163, no. 16, pp. 122–131, 2013.

[29] Z. Q. Zhang, H. Zhang, Y. T. Tan, and H. Y. Yang, "Natural wind utilization in the vertical shaft of a super-long highway tunnel and its energy saving effect," *Building and Environment*, vol. 145, pp. 140–152, 2018.

[30] C. P. Zhang, Y. J. Yue, and Y. Cai, "Influence of pipeline leakage range on ground deformation and failure during shallow tunnelling," *Chinese Journal of Rock Mechanics and Engineering*, vol. 34, no. 2, pp. 392–400, 2015.

[31] W. C. Cheng, J. C. Ni, and Y. H. Cheng, "Alternative shoring for mitigation of pier-foundation excavation disturbance to an existing freeway," *Journal of Performance of Constructed Facilities*, vol. 31, no. 5, 2017.

[32] C. Liu, Z. Lv, C. Zhu, G. Bai, and Y. Zhang, "Study on calculation method of long term deformation of RAC beam based on creep adjustment coefficient," *KSCE Journal of Civil Engineering*, vol. 23, no. 1, pp. 260–267, 2019.

[33] G. Zheng, X. Dai, and Y. Diao, "Parameter analysis of water flow during EPBS tunnelling and an evaluation method of spewing failure based on a simplified model," *Engineering Failure Analysis*, vol. 58, pp. 96–112, 2015.

[34] G. Zheng, X.-s. Zhang, Y. Diao, and H.-y. Lei, "Experimental study on grouting in underconsolidated soil to control excessive settlement," *Natural Hazards*, vol. 83, no. 3, pp. 1683–1701, 2016.

[35] Y. W. Zhang, X. L. Weng, Z. P. Song, and Y. F. Sun, "Modeling of loess soaking induced impacts on metro tunnel using water soaking system in centrifuge," *Geofluids*, vol. 2019, Article ID 5487952, 14 pages, 2019.

[36] R. Qiao, Z. Shao, F. Liu, and W. Wei, "Damage evolution and safety assessment of tunnel lining subjected to long-duration fire," *Tunnelling and Underground Space Technology*, vol. 83, pp. 354–363, 2019.

[37] X. Luo, D. Li, and S. Zhang, "Traffic Flow Prediction in Holidays Based on DFT and SVR," *Journal of Sensors*, vol. 2019, Article ID 6461450, 9 pages, 2019.

[38] Z.-F. Wang, J. S. Shen, and W.-C. Cheng, "Simple method to predict ground displacements caused by installing horizontal jet-grouting columns," *Mathematical Problems in Engineering*, vol. 2018, Article ID 1897394, 11 pages, 2018.

[39] Z. J. Zhou, C. N. Ren, G. J. Xu, H. C. Zhan, and T. Liu, "Dynamic failure mode and dynamic response of high slope using shaking table test," *Shock and vibration*, vol. 2019, Article ID 4802740, 15 pages, 2019.

[40] D. M. Zhang, L. X. Ma, J. Zhang, P. Y. Hicher, and C. H. Juang, "Ground and tunnel responses induced by partial leakage in saturated clay with anisotropic permeability," *Engineering Geology*, vol. 189, pp. 104–115, 2015.

[41] D. M. Zhang, Z. K. Huang, Z. Y. Yin, L. Z. Ran, and H. W. Huang, "Predicting the grouting effect on leakage-induced tunnels and ground response in saturated soils," *Tunnelling and Underground Space Technology*, vol. 65, pp. 76–90, 2017.

[42] Y. Luo, J. Chen, B. Liu, L. Chen, and J. Xie, "Analysis of pipe-roof in tunnel exiting portal by the foundation elastic model," *Mathematical Problems in Engineering*, vol. 2017, Article ID 9387628, 12 pages, 2017.

[43] H. Yu, C. Cai, A. Bobet, X. Zhao, and Y. Yuan, "Analytical solution for longitudinal bending stiffness of shield tunnels," *Tunnelling and Underground Space Technology*, vol. 83, pp. 27–34, 2019.

[44] E. J. Britton and P. J. Naughton, "The arching phenomena observed in experimental trap door model tests," in *Geo-Frontiers 2011*, pp. 788–797, Dallas, TX, USA, 2011.

[45] L. P. Li, S. C. Li, and Q. S. Zhang, "Study of mechanism of water inrush induced by hydraulic fracturing in karst tunnels," *Rock and Soil Mechanics*, vol. 31, no. 2, pp. 523–528, 2010.

[46] S. C. Li, J. Wu, Z. H. Xu, and L. P. Li, "Unascertained measure model of water and mud inrush risk evaluation in karst tunnels

and its engineering application," *KSCE Journal of Civil Engineering*, vol. 21, no. 4, pp. 1170–1182, 2017.

[47] B. Liu, Z. Liu, S. Li, K. Fan, L. Nie, and X. Zhang, "An improved time-lapse resistivity tomography to monitor and estimate the impact on the groundwater system induced by tunnel excavation," *Tunnelling and Underground Space Technology*, vol. 66, pp. 107–120, 2017.

[48] J. Zhang, S. Li, L. Li et al., "Grouting effects evaluation of water-rich faults and its engineering application in Qingdao Jiaozhou Bay Subsea Tunnel, China," *Geomechanics and Engineering*, vol. 12, no. 1, pp. 35–52, 2017.

[49] X. Guo, J. R. Chai, Y. Qin, Z. G. Xu, Y. N. Fan, and X. W. Zhang, "Mechanism and Treatment Technology of Three Water Inrush Events in the Jiaoxi River Tunnel in Shaanxi, China," *Journal of Performance of Constructed Facilities*, vol. 33, no. 1, article 04018098, p. 12, 2019.

[50] Y. Luo, J. Chen, H. Wang, and P. Sun, "Deformation rule and mechanical characteristics of temporary support in soil tunnel constructed by sequential excavation method," *KSCE Journal of Civil Engineering*, vol. 21, no. 6, pp. 2439–2449, 2017.

[51] J. Wang, Z. Ren, Z. Song, R. Huo, and T. Yang, "Study of the effect of micro-pore characteristics and saturation degree on the longitudinal wave velocity of sandstone," *Arabian Journal of Geosciences*, 2019, in press.

[52] J. Qiu, X. Wang, J. Lai, Q. Zhang, and J. Wang, "Response characteristics and preventions for seismic subsidence of loess in Northwest China," *Natural Hazards*, vol. 92, no. 3, pp. 1909–1935, 2018.

[53] X. Luo, L. Niu, and S. Zhang, "An algorithm for traffic flow prediction based on improved SARIMA and GA," *KSCE Journal of Civil Engineering*, vol. 22, no. 10, pp. 4107–4115, 2018.

[54] H. J. Zhang, Z. Z. Wang, F. Lu, G. Y. Xu, and W. G. Qiu, "Analysis of the displacement increment induced by removing temporary linings and corresponding countermeasures," *Tunnelling and Underground Space Technology*, vol. 73, pp. 236–243, 2018.

[55] Z. Zhang, H. Li, H. Yang, and B. Wang, "Failure modes and face instability of shallow tunnels under soft grounds," *International Journal of Damage Mechanics*, 2018, in press.

[56] E. Buckingham, "On physically similar systems; illustrations of the use of dimensional equations," *Physics Review*, vol. 4, no. 4, pp. 345–376, 1914.

[57] L. Russo, M. Sorrentino, P. Polverino, and C. Pianese, "Application of buckingham π theorem for scaling-up oriented fast modelling of proton exchange membrane fuel cell impedance," *Journal of Power Sources*, vol. 353, pp. 277–286, 2017.

[58] X. Li and Z. Shao, "Investigation of Macroscopic Brittle Creep Failure Caused by Microcrack Growth Under Step Loading and Unloading in Rocks," *Rock Mechanics and Rock Engineering*, vol. 49, no. 7, pp. 2581–2593, 2016.

[59] Q. Yan, Y. Xu, W. Zhang, P. Geng, and W. Yang, "Numerical analysis of the cracking and failure behaviors of segmental lining structure of an underwater shield tunnel subjected to a derailed high-speed train impact," *Tunnelling and Underground Space Technology*, vol. 72, pp. 41–54, 2018.

[60] X. Nie, X. Wei, X. Li, and C. Lu, "Heat treatment and ventilation optimization in a deep mine," *Advances in Civil Engineering*, vol. 2018, Article ID 1529490, 12 pages, 2018.

[61] X. Z. Li, X. L. Qu, C. Z. Qi, and Z. S. Shao, "A unified analytical method calculating brittle rocks deformation induced by crack growth," *International Journal of Rock Mechanics and Mining Sciences*, vol. 113, pp. 134–141, 2019.

[62] R. Ren, D. Yu, L. Wang, K. Wang, H. Wang, and S. Y. He, "Typhoon triggered operation tunnel debris flow disaster in coastal areas of SE China," *Geomatics, Natural Hazards and Risk*, vol. 10, no. 1, pp. 562–575, 2019, in press.

[63] Y. J. Zhang, X. Wang, Q. G. Liang, D. J. Jiang, and X. N. Ma, "Development of model test similar material of collapsible loess," *Chinese Journal of Rock Mechanics and Engineering*, vol. 32, no. 2, pp. 4019–4024, 2013.

[64] Z. Zhang, X. Shi, B. Wang, and H. Li, "Stability of NATM tunnel faces in soft surrounding rocks," *Computers and Geotechnics*, vol. 96, pp. 90–102, 2018.

[65] Y. Li, Y. Yang, H.-S. Yu, and G. Roberts, "Principal stress rotation under bidirectional simple shear loadings," *KSCE Journal of Civil Engineering*, vol. 22, no. 5, pp. 1651–1660, 2018.

[66] J. Wang, Z. Song, B. Zhao, X. Liu, J. Liu, and J. Lai, "A study on the mechanical behavior and statistical damage constitutive model of sandstone," *Arabian Journal for Science and Engineering*, vol. 43, no. 10, pp. 5179–5192, 2018.

[67] Y.-Q. Wang, Z.-F. Wang, and W.-C. Cheng, "A review on land subsidence caused by groundwater withdrawal in Xi'an, China," *Bulletin of Engineering Geology and the Environment*, pp. 1–13, 2018.

[68] ABAQUS, *Abaqus Scripting User's Manual, Version 6.10*, ABAQUS, Inc., Johnston, RI, USA, 2010.

[69] Y. Li, S. Xu, H. Liu, E. Ma, and L. Wang, "Displacement and stress characteristics of tunnel foundation in collapsible loess ground reinforced by jet grouting columns," *Advances in Civil Engineering*, vol. 2018, Article ID 2352174, 16 pages, 2018.